On the Use of Doppler Radar–Derived Wind Fields to Diagnose the Secondary Circulations of Tornadoes

DAVID S. NOLAN

Rosenstiel School of Marine and Atmospheric Science, University of Miami, Miami, Florida

(Manuscript received 13 July 2012, in final form 29 October 2012)

ABSTRACT

A number of studies in recent years have used wind fields derived from portable Doppler radars in combination with the ground-based velocity track display (GBVTD) technique to diagnose the primary (tangential) and secondary (radial and vertical) circulations in tornadoes. These analyses indicate very strong vertical motions in the vortex core, in some cases with updrafts and downdrafts exceeding 100 m s^{-1}. In addition, many of the analyses indicate strong radial outflow at low levels and in the vicinity of the low-level tangential wind maximum. This paper shows that strong outward motion at this location cannot be consistent with a tornado circulation that lasts more than a few minutes. In addition, using data from numerical simulations as truth, it is shown that using observed radial velocities to diagnose vertical velocities greatly overestimates the intensity of downward motion in the core for two reasons: neglect of the mass flux into the core through the swirling boundary layer, and the likely positive bias in low-level radial velocities due to the centrifuging of debris. Possible methods for accounting for these errors are briefly discussed.

1. Introduction

As discussed in the recent review by Rotunno (2013), much of what we believe to understand about the inner-core dynamics of tornadoes comes from laboratory models, numerical simulations, and mathematical theory of swirling boundary layers. However, in recent years the development of two observational methods, one mathematical and one technological, have seemed to make it possible to finally directly diagnose the three-dimensional wind field inside significant tornadoes. These two methods are, respectively, the ground-based velocity track display (GBVTD) technique, as developed by Lee et al. (1999, 2000; also Lee and Marks 2000), and the use of portable Doppler radars (Bluestein et al. 1995; Wurman et al. 1997).

GBVTD was originally developed to diagnose the wind fields of tropical cyclones that come within range of a single Doppler radar. Using the assumption that the wind field is dominated by a strong and fairly axisymmetric tangential wind field, and after diagnosing the center location and mean flow around the storm, GBVTD can (it is believed) provide usefully accurate profiles of the azimuthal-mean (axisymmetric) parts of the tangential (V) and radial (U) wind fields. By vertically integrating the radial divergence of U, Lee et al. (2000) derived estimates of the axisymmetric vertical velocity (W) fields in Typhoon Alex (1987), while Lee and Bell (2007) derived W fields in Hurricane Charley (2004).

Since the 1990s, portable Doppler radars have been used to derive radial profiles of U and V in tornadoes. At first, such analyses were restricted to U along the line of sight and through the center of the tornado and to V perpendicular to the line of sight and through the center. In a few cases, two portable Doppler radars have been deployed in range of a tornado so that the complete wind field could be accurately mapped (Wurman et al. 2007, 2010). However, as recently noted in Wakimoto et al. (2012), such instances are rare and do not typically provide sufficiently high spatial resolution to map the inner core of a tornado.

Bluestein et al. (2003) used GBVTD to derive profiles of axisymmetric U and V at a single height level through the Bassett, Nebraska, tornado of 1999. Of note is the fact that the radial inflow did not often reach the location of maximum V (hereafter, V_{max}, used interchangeably with the value of V_{max} or the radius–height location

Corresponding author address: David S. Nolan, RSMAS/MPO, 4600 Rickenbacker Causeway, Miami, FL 33149.
E-mail: dnolan@rsmas.miami.edu

DOI: 10.1175/JAS-D-12-0200.1

where it occurs), and there was instead radial outflow at V_{max}, even when the data was averaged over the period when the tornado was most intense (see their Fig. 5). As this configuration would be counter to expectations at the lowest levels,[1] they considered the sensitivity of the $U(r)$ retrieval to the vortex center location and the effects of outward centrifuging debris on the Doppler velocities as possible reasons. Similarly, GBVTD analyses at a single level by Tanamachi et al. (2007) of the Stockton, Kansas, tornado of 1999 also show positive U in the vicinity of V_{max} (see their Figs. 8 and 10). As will be discussed below, positive U can be expected along the vertical axis of maximum $V(r)$ above the level of V_{max} but this altitude cannot be known from a single-level analysis.

The Doppler-on-Wheels (DOW) developed by Wurman and collaborators allows for full volume scans and thus the possibility of retrieving the full U, V, and W fields as a function of radius and height. Lee and Wurman (2005) applied the GBVTD method to wind fields derived from a single portable Doppler radar deployed near the Mulhall, Oklahoma, tornado on 3 May 1999. The Mulhall tornado was large, with a radius of maximum winds (RMW) varying from 500 to 1000 m. Their analyses show peak winds of 70–80 m s^{-1} that are maximized at the lowest analysis level at $z = 50$ m; there is no indication of the boundary layer in which V would decrease toward the surface. In the later part of their analysis period the results show positive U (radial outflow) often emanating out from the center axis and flowing outward across the vertical axis of maximum V, which they correlated with the fact that the tornado was weakening and expanding at that time. In addition, strong downward motions in excess of 30 m s^{-1} were identified aloft near the center axis of the vortex.

Kosiba et al. (2008) used a simplified version of the GBVTD technique proposed by Dowell et al. (2005) to derive axisymmetric U, V, and W for a tornado near Harper, Kansas, in 2004. While radial inflow does penetrate to the center at the lowest level (50 m) during the earlier phase of the analysis (their Fig. 3a), the later phase shows radial outflow at this level (their Fig. 3b), during which the peak values of V are increasing in time and appear to be maximized even further aloft around $z = 100$ m (their Fig. 3d).

Kosiba and Wurman (2010) used the full GBVTD method to compute volumes of U, V, and W for the Spencer, South Dakota, tornado of 1998. Their Fig. 5 shows persistent and strong (4–10 m s^{-1}) radial outflow at the lowest analysis level ($z = 40$ m) that is often coincident with the location of maximum V at that level. In addition, their Fig. 6 shows very strong downdraft velocities (peak values from 50 to 100 m s^{-1}) flowing down from the upper part of the analysis region and then turning outward to form the strong radial outflow at the lowest levels.

To summarize, a number of studies using GBVTD to derive instantaneous and mean fields of U, V, and W in tornadoes have found radial outflow at the lowest levels that is also coincident with the location of V_{max}. Such a flow configuration is at odds with what we believe (from theory and numerical simulations) should be true about tornadoes and other swirling boundary layers. As discussed in Dowell et al. (2005) and more recently by Wakimoto et al. (2012), one explanation for the unexpected outward flow is that the Doppler radar analysis is in fact detecting the outward motion of larger debris under the influence of centrifugal accelerations. Using the numerical method developed by Dowell et al. (2005), Wakimoto et al. (2012) estimated the likely outward speeds of such particles and used these to correct the U field diagnosed from GBVTD for the Lagrange, Wyoming, tornado of 2009. Along with improving the U field, this correction also made drastic changes to the W field computed from radial divergence.

In this paper we will further explore the limitations of computing W from U that is derived from GBVTD or even dual-Doppler techniques. Our approach is to use the output of numerical simulations as a ''perfect'' dataset, and then to consider the effects of errors in the analysis process. In addition to the effects of centrifuging debris, we also consider the effect of neglecting the mass flux of the radial inflow in the tornado boundary layer, which appears to be often less than 100 m deep. Section 2 of this paper examines the wind fields from KW10. Section 3 describes the numerical simulations that provide the perfect data, and then shows how neglecting the boundary layer mass flux and/or not accounting for centrifuging particles can lead to highly erroneous vertical velocity fields. Conclusions and some possible solutions to these problems are discussed in section 4.

2. Examination of wind fields previously diagnosed with GBVTD

To evaluate the physical consistency of published, GBVTD-derived tornado wind fields, we consider the wind fields of Kosiba and Wurman (2010, hereafter KW10). This set of wind analyses shows the U, V, and W wind fields of the tornado that passed through Spencer,

[1] The altitude above ground level to which their wind analyses correspond is not stated in either Bluestein et al. (2003) or Tanamachi et al. (2007).

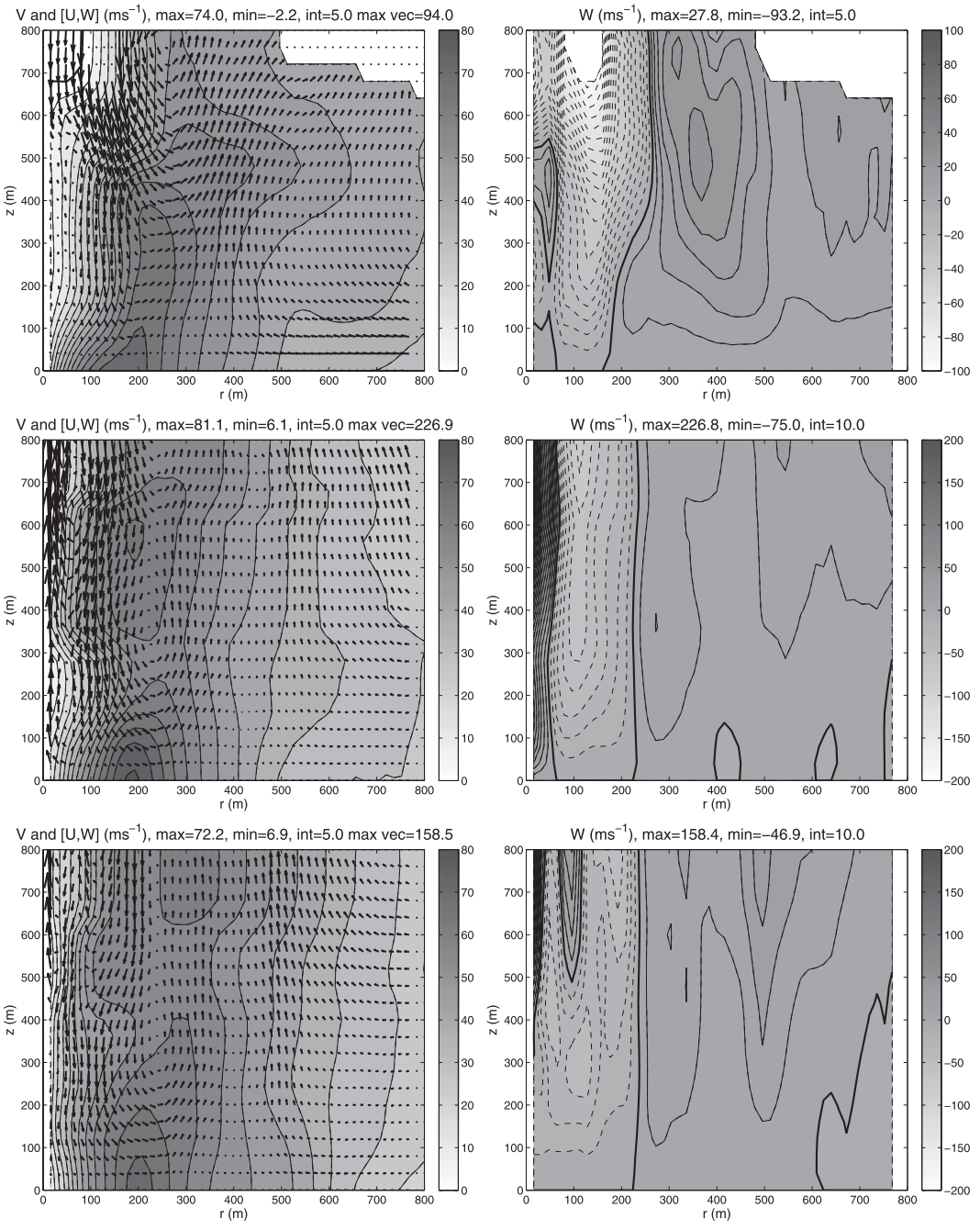

FIG. 1. Axisymmetric wind fields from KW10 at (top) 0134:23, (middle) 0138:23, and (bottom) 0140:02 UTC 31 May 1998. (left) V (shaded) with $[U, W]$ vectors overlaid; (right) W (shaded) only. Dashed contours indicate negative values, and the zero contour is thickened. The vectors are scaled so that a vector that reaches from one grid point to the next indicates 40 m s^{-1}. Contour intervals and extreme values are indicated at the top of each plot.

South Dakota, in the evening hours of 30 May 1998. Figure 6 of KW10 shows the wind fields in terms of contours and shading for V and curved, elongated vectors indicating the magnitude of the meridional wind vector $[U, W]$ as well as, presumably, the paths that parcels would have taken if the flow were frozen in time. Using data provided by Kosiba and Wurman, Fig. 1 shows the same data for Figs. 6b, 6f, and 6g of KW10, corresponding to 0134:23, 0138:23, and 0140:02 UTC 31 May 1998, respectively. In addition, Fig. 1

shows shaded contour plots of W only for the same times. The KW10 data grid is evenly spaced, with 50 grid points in the radial direction from $r = 16$ to 800 m, and 21 grid points in the vertical direction from $z = 0$ to 800 m.

The plots on the left side of Fig. 1 have common features that are also shared by Figs. 6c and 6h (0135:20 and 0140:49 UTC) of KW10: each has an intense wind maximum in the range of 60 to 80 m s^{-1} at the lowest level. In KW10, these are depicted to be at $z = 0$ m above ground (i.e., the surface), even though the effective observation level of the lowest radar elevation angle was about 20 m. The KW10 data at $z = 0$ m are generated from linear extrapolation of the data above (K. Kosiba 2012, personal communication). In addition, all the analyses show very strong downdrafts coming down through the core of the vortex, just inside the RMW at each level. In Fig. 1b, the peak downdraft speed is -93 m s^{-1}. Figure 1d shows a peak downdraft[2] of -75 m s^{-1} and a peak updraft near the central axis of $+226$ m s^{-1}. For Fig. 1f, the peak speeds are -47 and $+158$ m s^{-1}. In all three cases these extreme updrafts are restricted to very close to $r = 0$, inside the annulus of the strongest downdraft, which in turn is located inside the larger annulus of the broader, primary tornado updraft.

Such a configuration of concentric updrafts and downdrafts would be highly unstable (see, e.g., Howard and Gupta 1962; Leibovich and Stewartson 1983; Nolan 2012). While such a flow configuration might appear briefly, the fact that it is persistent across many minutes of the GBVTD wind fields is concerning.[3] Using the KW10 data, we computed our own vertical velocities based on the radial mass flux:

$$W_{\mathrm{MF}} = -\int_0^z \frac{1}{r\rho}\frac{\partial}{\partial r}(r\rho U)\,dz, \tag{2.1}$$

where hereafter we assume that the density ρ can be treated as a constant, and we numerically solve (2.1) with the finite-difference scheme:

$$W_{\mathrm{MF}(i,j)} = W_{\mathrm{MF}(i,j-1)} - \frac{dz}{4dr}\frac{1}{r_i}[(ru)_{i+1,j} + (ru)_{i+1,j-1} - (ru)_{i-1,j} - (ru)_{i-1,j-1}]. \tag{2.2}$$

The quantity W_{MF} computed in this manner was found to be nearly identical to the W values provided from KW10, so we may presume their numerical method was similar.

In each case, the inner-core downdraft turns outward at low levels and flows outward through the local wind maximum near the surface. The peak values of U in the low-level outflow regions of Figs. 1a, 1c, and 1e are 10.0, 13.1, and 11.3 m s^{-1}, respectively, with peak values of U at the lowest level being 1.7, 8.0, and 7.7 m s^{-1}, respectively.

As discussed by Kepert (2001), there must be radial inflow at $V_{\max}$ in a swirling boundary layer. For the axisymmetric wind V,

$$\frac{\partial V}{\partial t} = -U\frac{\partial V}{\partial r} - W\frac{\partial V}{\partial Z} - \frac{UV}{r} + F_V, \tag{2.3}$$

where here F_V represents the effects of turbulent diffusion. The quantity F_V can be expected to be negative at $V_{\max}$. The gradients of V are also zero (or very small) at and around $V_{\max}$. Therefore, in order for $V_{\max}$ to be in a steady state or to at least remain near its peak value, U must be negative to balance the effects of diffusion. Numerical simulations of tornadoes, whether highly idealized (Fiedler 1994, 1998; Nolan and Farrell 1999; Nolan 2005) or more realistic large-eddy simulations (Lewellen et al. 1997, 2000), show weak radial inflow at and around the tangential wind maximum. Similarly, for hurricane boundary layers, both observational analyses (Bell and Montgomery 2008; Zhang et al. 2011) and numerical simulations (Zhang et al. 2001; Nolan et al. 2009) show radial inflow[4] at $V_{\max}$.

Outward radial velocity above $V_{\max}$ is shown in observational analyses and simulations of hurricanes and in numerical simulations of tornadoes. This flow is part of the second branch of the corner flow region, consisting of boundary layer air that has overshot the point of gradient wind balance, penetrated to smaller radius to achieve supergradient wind speed, and then is rebounding outward as it is simultaneously forced to rise because of mass convergence in the boundary layer. There is radial outflow across the vertical axis of the

[2] KW10 describes a peak downdraft speed at this time of about 60 m s^{-1}, but 75 m s^{-1} appears in the dataset, and is also reproduced by our own calculation of W from integrating the radial divergence.

[3] To be fair to KW10, they state that ''the precise magnitude of the retrieved vertical velocity values should be viewed with caution'' (p. 3078). They also cite the absence of the boundary layer inflow as a possible reason for exaggerating the intensity of the peak downdrafts. It is shown in the next section that this is indeed the case, but furthermore, the neglect of outward velocity of centrifuging debris contributes even more to this problem.

[4] As Kepert (2001) further discussed, in order to maintain radial inflow at $V_{\max}$, there must also be even stronger radial inflow either radially outward or below $V_{\max}$; observations and simulations show both are true.

RMW in this region, but there is also positive vertical advection of the faster winds from below. In most of the wind fields of KW10, the vertical motion around V_{max} is also downward or near zero.

If negative U near and around V_{max} is required to maintain steady-state intensity, positive U indicates weakening of the vortex. Given the analyzed fields, how fast should the Spencer tornado be weakening? Using the KW10 data, we use centered differences to compute the first three terms on the rhs of (2.3). Their sums are shown in Fig. 2. In each case, there is a local maximum in negative advective tendency above and radially inward of V_{max}, with negative values extending to the lowest level. (Data on each boundary have been suppressed.) The low-level negative maxima are -8.2, -12.0, and -7.6 m s^{-2}, with negative values of -3.2, -4.6, and -4.9 m s^{-2} at $z = 40$ m. These are large tendencies. For example, consider the low-level jet depicted in Fig. 1b. At the location of the -4.6 m s^{-2} tendency, $V = 76.2$ m s^{-1}. Therefore at this location the circulation would exponentially decay with a spindown time scale of about 16 s. At the negative tendency maximum of -12.0 m s^{-2}, the tangential wind speed with $V = 60$ m s^{-1} would decay away with a time scale of just 5 s. However, the data in Fig. 1e, which pertains to the Spencer tornado 99 s later, shows that the circulation has hardly weakened at all, and is nearly identical in structure.

The radial and vertical wind fields presented in KW10 are not consistent with a large body of knowledge derived from theory and numerical simulations of swirling boundary layers.

3. Assessing the GBVTD technique with perfect data

a. Numerical model and data processing

To identify possible sources of error in diagnosing secondary circulations in tornadoes with GBVTD, we use as ''perfect data'' the output of numerical simulations of tornado-like vortices. These data are generated from the model of Nolan and Farrell (1999). It solves the axisymmetric Navier–Stokes equations for an incompressible fluid in a finite, cylindrical domain, and produces tornado-like vortices very similar to those of Fiedler (1994, 1998, 2009) and Dowell et al. (2005). The model domain and forcing are the same as in Nolan (2005): a fixed buoyancy forcing function is placed at the center axis of a cylindrical domain in the region $0 \le r \le 6000$ m, $0 \le z \le 6000$ m. The computational grid is evenly spaced with 128×256 points, such that $\Delta r = 46.88$ m and $\Delta z = 23.44$ m. The upper, outer, and lower

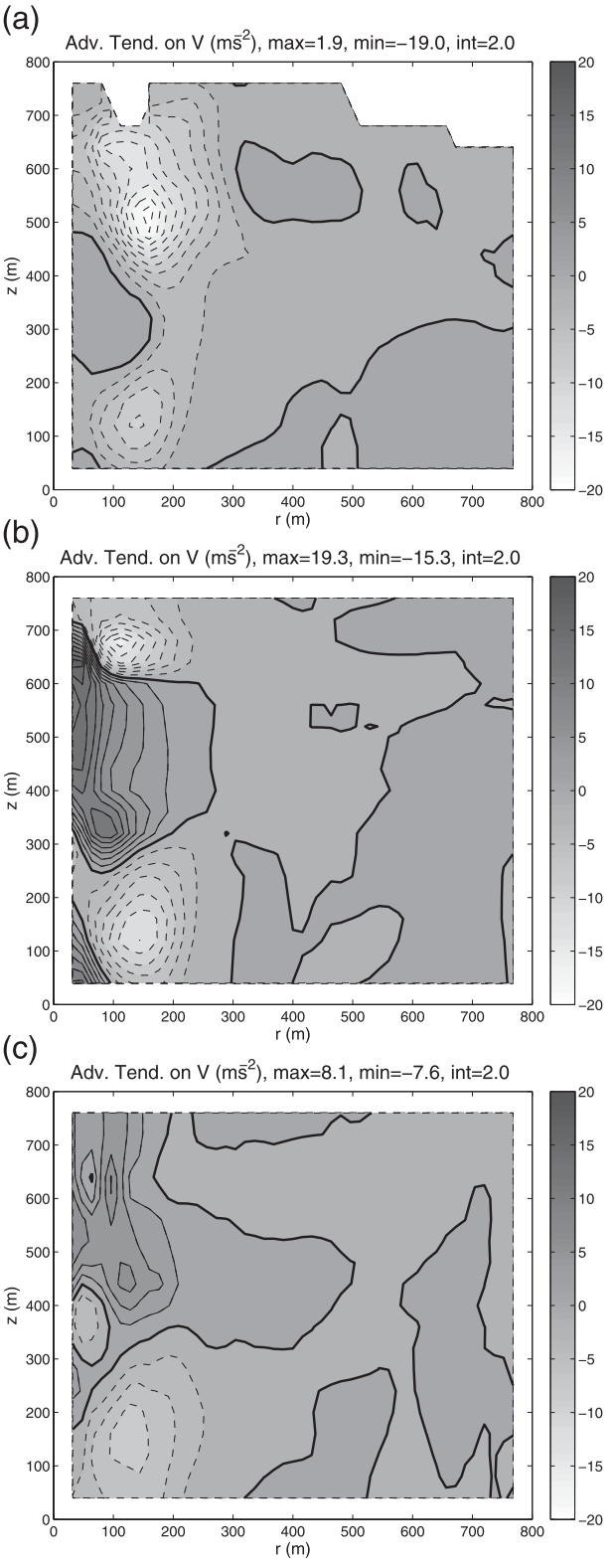

FIG. 2. Tendencies on the axisymmetric V due to the sum of radial and vertical advection terms as computed from the KW10 wind fields for (a) 0134:23, (b) 0138:23, and (c) 0140:02 UTC 31 May 1998.

boundaries and the initial flow are set to solid-body rotation[5] at a specified angular velocity Ω. The boundary conditions on the upper, outer, and lower boundaries are impermeable and no slip, except when a bulk-drag law formula is used to define the stress at the lower boundary. At $r = 0$, $U = V = 0$ and $\partial W/\partial r = 0$.

The vertical forcing function forces convergence of the fluid at low levels. This leads at first to the development of a very intense, transient vortex, followed by adjustment to a quasi-steady state with axisymmetric oscillations (Fiedler 1994; Nolan and Farrell 1999; Nolan 2012).

We use output from two simulations. The first uses $\Omega = 0.002\ \mathrm{s}^{-1}$, an interior eddy viscosity of $\nu = 25\ \mathrm{m}^2\ \mathrm{s}^{-1}$, and a no-slip lower boundary condition, designated simulation NS. The second also uses $\Omega = 0.002\ \mathrm{s}^{-1}$ and $\nu = 25\ \mathrm{m}^2\ \mathrm{s}^{-1}$, but uses a bulk-drag law lower boundary condition with surface roughness $z_0 = 0.2$ m, designated simulation BD. The parameters have been chosen to produce tornado-like vortices that are similar in size and intensity to the Spencer tornado. Each simulation was integrated for 1 h, during which both vortices reached quasi-steady states, and the model output was saved every 20 s for the last 10 min.

The model output (either time means or instantaneous fields, as specified below) is mapped onto an identical grid as in KW10 using bilinear interpolation. The values of U, V, and W from the numerical model lie on a cell-centered grid, so the lowest model level with data is at $z = 11.72$ m. Horizontal velocities at $z = 0$ on the KW10 grid are set to $U = 0$ and $V = \Omega r$ for simulation NS, or are set by second-order extrapolation for simulation BD.

b. Simulation NS

Time means over the last 10 min of simulation NS, interpolated onto the KW10 grid, are shown in Fig. 3. The flow structure is similar to the ''medium swirl'' structures produced in many previous simulations (Fiedler 1994; Lewellen et al. 2000; Nolan 2005), with strong radial inflow feeding into the corner region, just reaching the center axis, rebounding outward above $V_{\max}$, and then turning upward to form the main column of the vortex.

Also shown in Fig. 3d is W_{MF} as computed from (2.2). While W_{MF} is a fairly good approximation to W in terms of the overall structure, the peak local errors are not small, with maximum positive and negative errors of 3.1 and $-9.3\ \mathrm{m\ s}^{-1}$. The peak updraft is underestimated and the peak central downdraft is overestimated. The volume-weighted root-mean-square (RMS) error is $4.4\ \mathrm{m\ s}^{-1}$. These large differences are due to the interpolation of the model data onto the KW10 grid and the inherent errors in computing radial divergence at small radius. The RMS error can be improved if the vertical grid spacing is decreased to more closely match the numerical model. For example, if the vertical resolution is doubled, it decreases to $1.3\ \mathrm{m\ s}^{-1}$. The peak errors, however, do not improve.

Now let us consider the consequences of neglecting the lowest levels of the boundary layer. We repeat the calculation of W_{MF}, but we treat the first grid point above the surface ($z = 40$ m) as the lowest level, so that $W_{\mathrm{MF}} = 0$ there, and integrate upward as before. The result of this calculation is shown in Fig. 4a. The errors are increased, and the peak updrafts are now underestimated by over $10\ \mathrm{m\ s}^{-1}$. Figure 4b shows the results of beginning the integration at $z = 80$ m. In this case, the updrafts are underestimated further, and an anomalously large downdraft appears at $z = 400$ m. The total downdraft mass flux entering the upper part of the domain has increased by a factor of 5 over the original value.

Neglecting the boundary layer leads to errors in W_{MF} but does not explain the very large negative values of W_{MF} in the inner core as computed by KW10. Following Wakimoto et al. (2012), we consider the effects of positive bias in U caused by outward centrifuging debris in the wind field. Using the results of Dowell et al. (2005) and Wakimoto et al. (2012) for guidance, we propose the following simplified function for the biased radial wind field U_{mod}:

$$U_{\mathrm{mod}} = U + U_{\mathrm{bias}} = U + C_{\max}\frac{V^2/r}{\max(V^2/r)}, \quad (3.1)$$

where $C_{\max}$ is a specified maximum flow-relative outward velocity for the relevant debris. In other words, U_{mod} is equal to U plus a positive bias that is proportional to the centripetal force at each location, scaled to have value $C_{\max}$ at the location of maximum centripetal force.

We consider $C_{\max} = 4.0\ \mathrm{m\ s}^{-1}$ and $C_{\max} = 8.0\ \mathrm{m\ s}^{-1}$. For the latter value, U_{bias} and U_{mod} are shown in Figs. 4c and 4d, respectively. The results of calculating W_{MF} with

[5] Setting the boundaries (including the ground) into solid-body rotation is a device for restoring angular momentum to the fluid in the domain. Fiedler (1994, 1998) achieved the same effect by using a Coriolis force. This allows such simulations to maintain a steady-state circulation. Without this forcing, the angular momentum supply to the vortex decreases after some time, leading to large structural changes. Having the lower boundary in solid-body rotation does cause small changes to the boundary layer flow, but for the rotation rate used here the V velocity of the lower boundary underneath the RMW is just $0.4\ \mathrm{m\ s}^{-1}$.

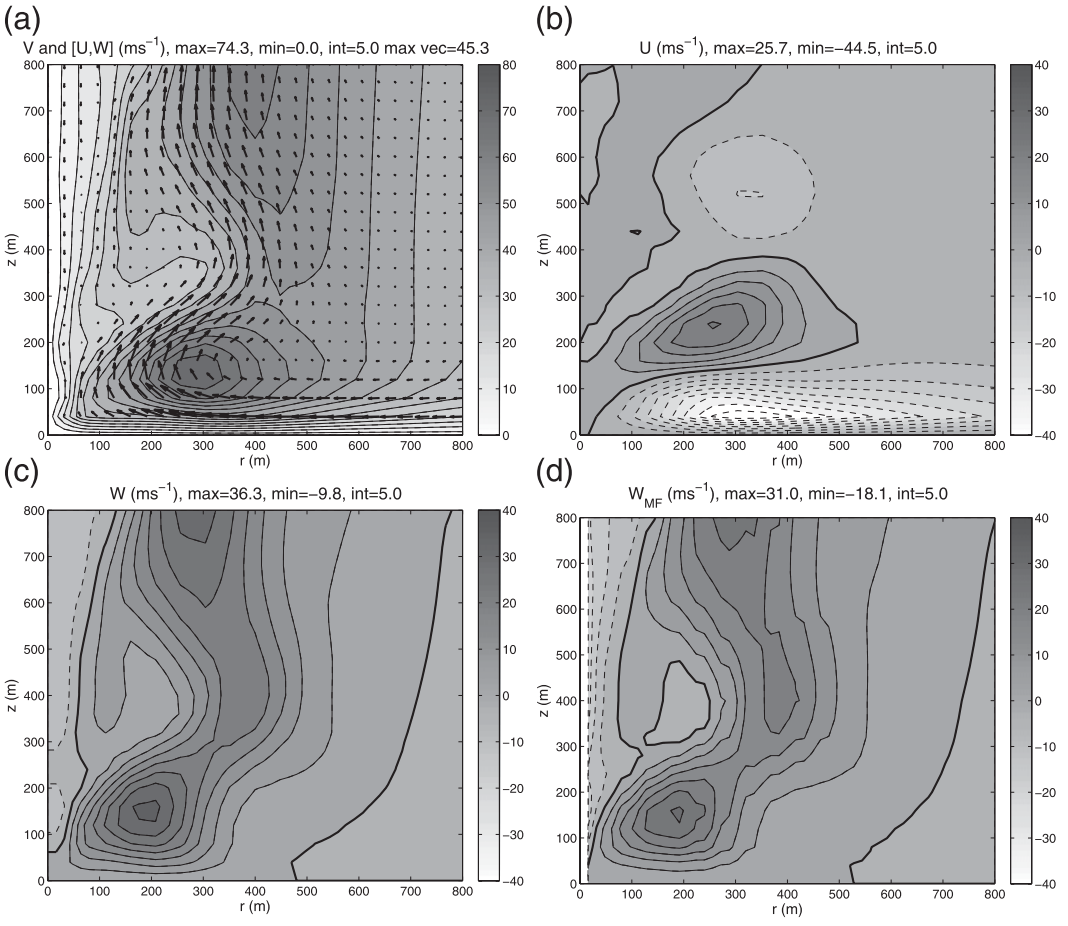

FIG. 3. Time-mean simulated wind fields for the axisymmetric numerical simulation NS, interpolated onto the KW10 analysis grid: (a) V with overlaid vectors of $[U, W]$, (b) U, (c) W, and (d) W_{MF} computed from the radial divergence of U. Dashed contours are negative, the zero contour is thickened, and vectors are scaled so that a vector reaching from one grid point to the next corresponds to 40 m s^{-1}. Extreme values and contour intervals are indicated at the top of each plot.

U_{mod} for these two values of C_{max} are shown in Figs. 4e and 4f. For $C_{max} = 4.0$ m s^{-1}, the peak downdraft speed increases from -18 to -38 m s^{-1}; for $C_{max} = 8.0$ m s^{-1}, it increases further to -61 m s^{-1}. Interestingly, the structure and intensity of the updrafts are not radically changed.

c. The BD simulation

The results above suggest that neglecting the boundary layer mass flux and the outward motion can severely bias calculations of W_{MF}. However, we should consider the possibility that the errors are amplified by the particular structure of the simulated tornado. Using a no-slip lower boundary condition leads to what is probably an unrealistically intense secondary circulation, with overly strong radial inflow and outflow. The time-mean flow of simulation BD is shown in Fig. 5. The inflow layer is slightly shallower and significantly weaker, the wind maximum is closer to the surface, the peak updraft speed is about one-third less, and the total updraft mass flux (not shown) is about half as large as for NS. The weaker secondary circulation leads to a significant decrease in the baseline error for W_{MF} (Fig. 5d), with peak vertical velocities errors of 3.6 and -5.8 m s^{-1}. The volume-weighted RMS error is substantially less than for NS—just 0.2 m s^{-1}.

Figure 6 shows for BD the results of identical calculations shown in Fig. 4 for NS. Neglecting the first and second levels of the inflow layer causes the peak updraft to be substantially decreased as well as shifted radially outward. Adding U_{bias} to U causes drastic increases in the width and intensity of the inner-core downdraft, especially for $C_{max} = 8.0$ m s^{-1}, which is very similar to the peak values of U_{bias} used by Wakimoto et al. (2012; see their Fig. 9).

The calculations shown above used time-mean wind fields over 10 min of each simulation, which produces

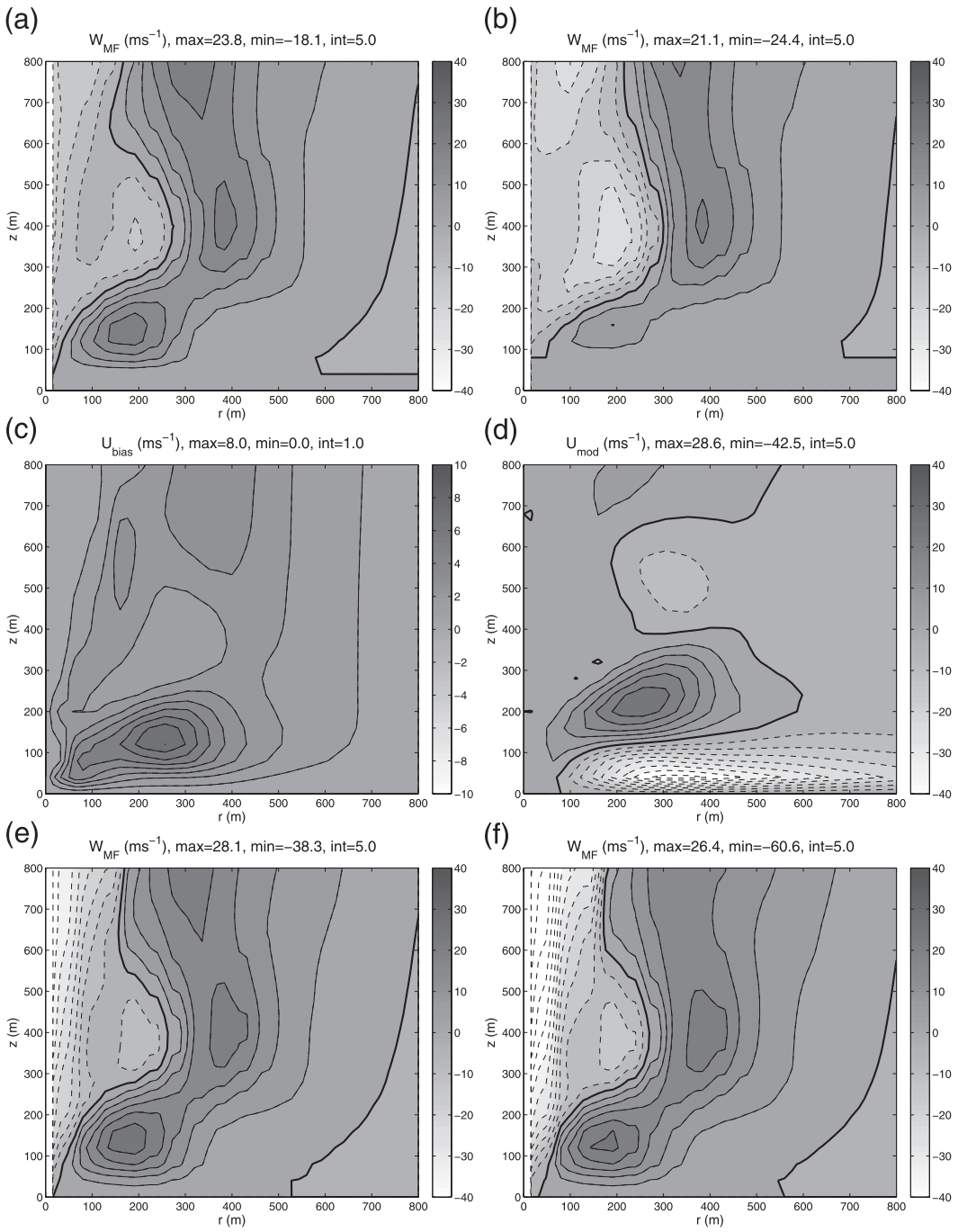

FIG. 4. Results from modified calculations for W_{MF} with simulation NS: (a) integration beginning at $z = 40$ m, (b) integration beginning at $z = 80$ m, (c) bias of U from outward centrifuging debris for $C_{max} = 8$ m s^{-1}, (d) result of modifying U with this bias, (e) W_{MF} calculated with $C_{max} = 4$ m s^{-1}, and (f) W_{MF} calculated with $C_{max} = 8$ m s^{-1}.

rather smooth wind fields. Not surprisingly, the discrepancies are even worse when an instantaneous snapshot of the wind field is used. Figure 7 shows the wind field from the BD simulation at $t = 3464$ s. The instantaneous flow shows a secondary maximum in V at $z = 500$ m; similar secondary maxima in V were shown in Wakimoto et al. (2012; see their Fig. 4), although at lower altitude. Figure 7 also shows two calculations for W_{MF}. The first (Fig. 7c) neglects the radial flow below $z = 40$ m, and thus shifts the low-level updraft outward

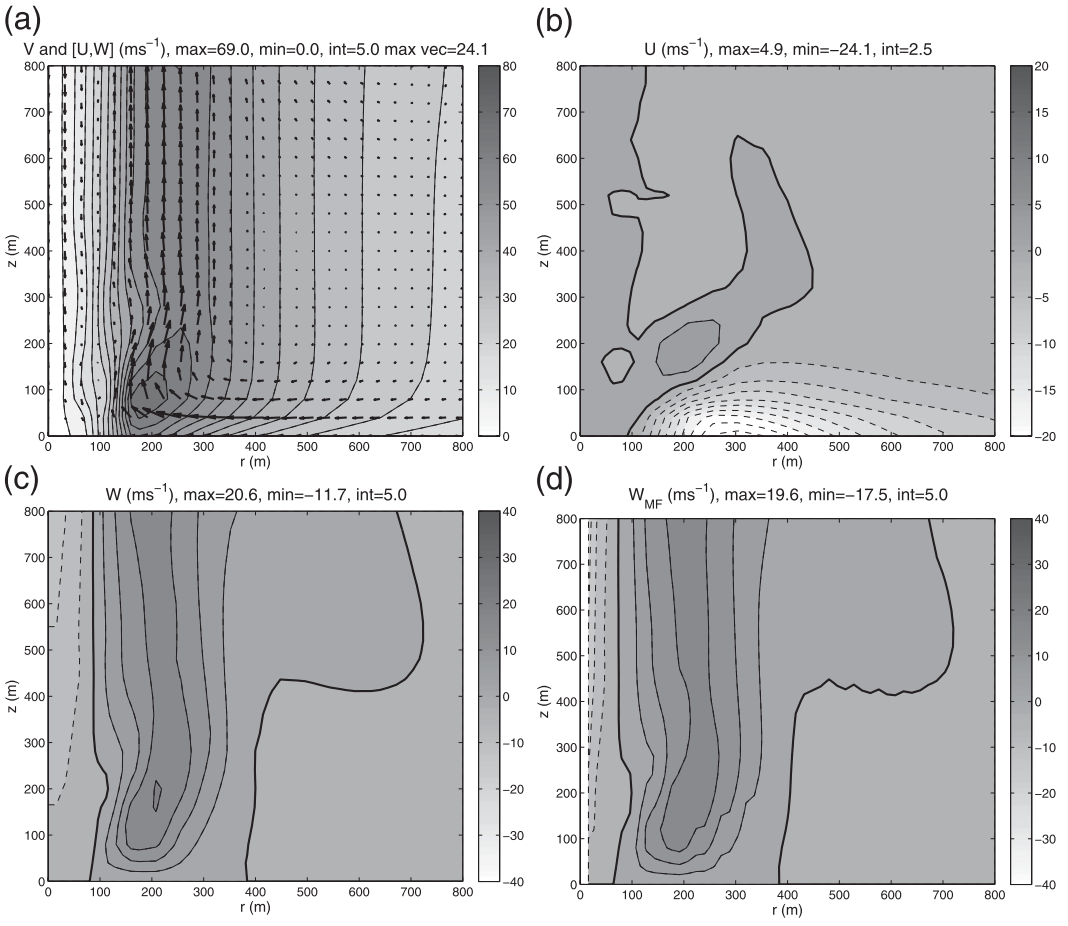

FIG. 5. As in Fig. 3, but for simulation BD; vectors are now scaled by 20 m s^{-1} and the contour interval for U has changed from 5.0 to 2.5 m s^{-1}.

and underestimates the updraft intensity. The second (Fig. 7d) neglects the lowest 40 m and also uses U_{mod} with $C_{\max} = 4.0$ m s^{-1}. The resulting W_{MF} has a further weakened updraft, a much wider downdraft region, and peak downdraft speed of -52 m s^{-1}. Figure 7d has some similarities to the W fields of KW10 (Figs. 1b,d,f).

4. Conclusions

This study has explored the extent to which Doppler radar–derived wind fields in tornadoes can be trusted, both in terms of their physical plausibility and whether derived radial winds can be used to accurately infer the simultaneous vertical velocity field. First, we examined the wind fields from the dataset of KW10. These fields contain extremely large vertical velocities (e.g., greater than 100 m s^{-1}) of alternating signs in concentric annuli in the core of the tornado vortex. In addition, they show radially outward motion at the location of $V_{\max}$. Such a configuration could not exist for more than a few seconds before the tornado would weaken drastically.

Using the output of idealized numerical simulations, we explored the extent to which observed radial velocities can be used to reliably diagnose vertical velocities. Even using ''perfect'' data with the numerically simulated wind fields linearly interpolated onto an analysis grid of different resolution, the resulting calculations were found to have peak errors ranging from 5 to 10 m s^{-1}. We assessed the consequences of not being able to account for the mass flux associated with the radial inflow in the lowest 80 or 40 m of the boundary layer. The effect is to weaken the diagnosed wind speed (and mass flux) of the primary updraft in the tornado, as well as to shift the location of the updraft radially outward, and to make the downdraft in the core slightly wider.

The effects of a positive bias in U caused by debris centrifuging outward in the tornado wind fields were also considered. Small peak values of the outward bias

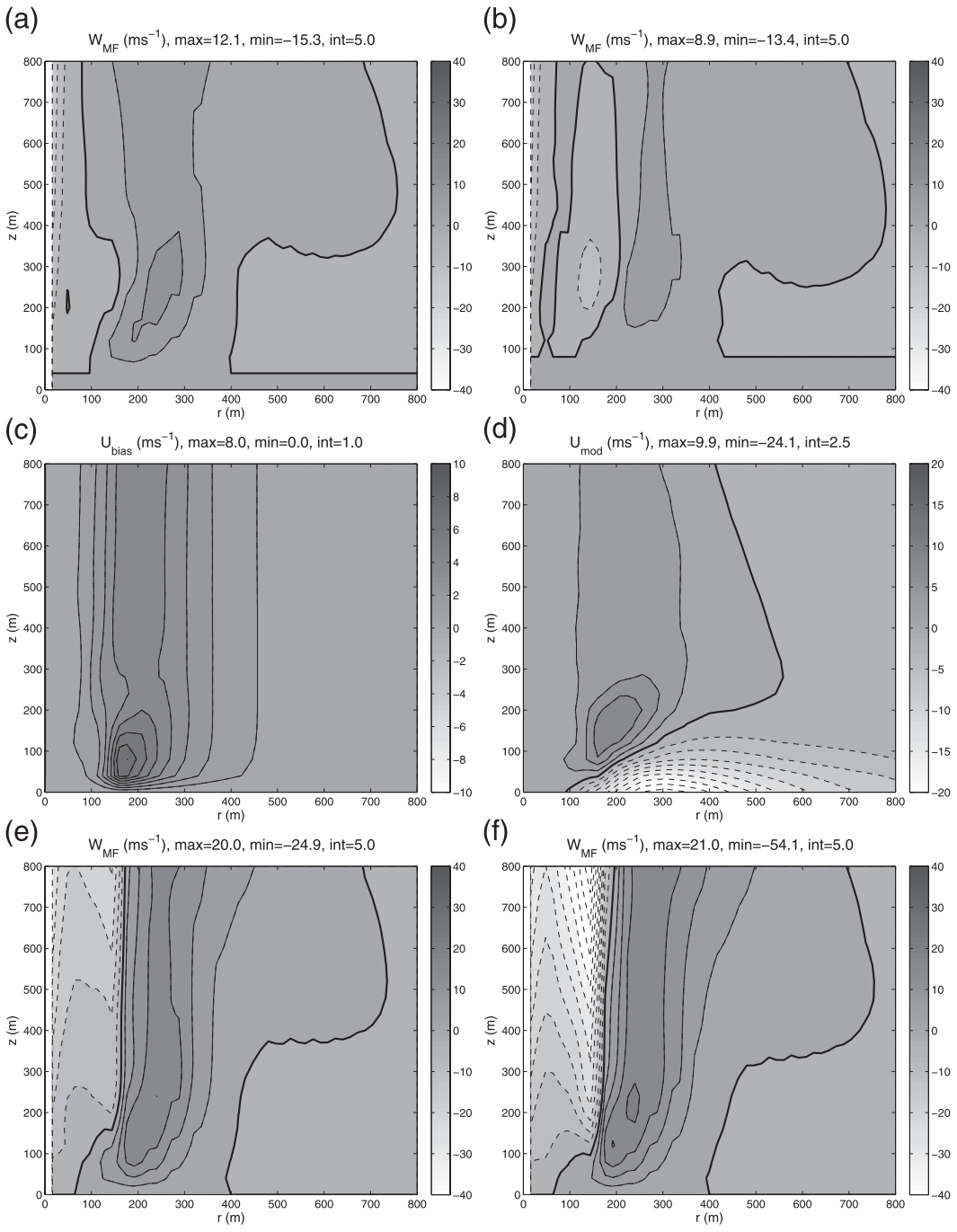

FIG. 6. As in Fig. 4, but for simulation BD.

(C_{max}) such as 4 m s^{-1} cause a significant increase in the peak downdraft velocity (and mass flux) of the diagnosed inner-core downdraft. A larger value of C_{max} = 8 m s^{-1}, similar to that used by Wakimoto et al. (2012), leads to even more extreme (and less likely) downdraft speeds. Finally, a "most probable" case, using an instantaneous wind field from the BD simulation, neglecting the mass flux in the lowest 40 m, and using C_{max} = 4 m s^{-1}, was shown to produce a W field with underestimated updraft speeds at low levels and a 52 m s^{-1} downdraft in the vortex core.

It could be possible to account for each of these error mechanisms. In regards to the boundary layer mass flux, a number of studies have provided solutions for U and V

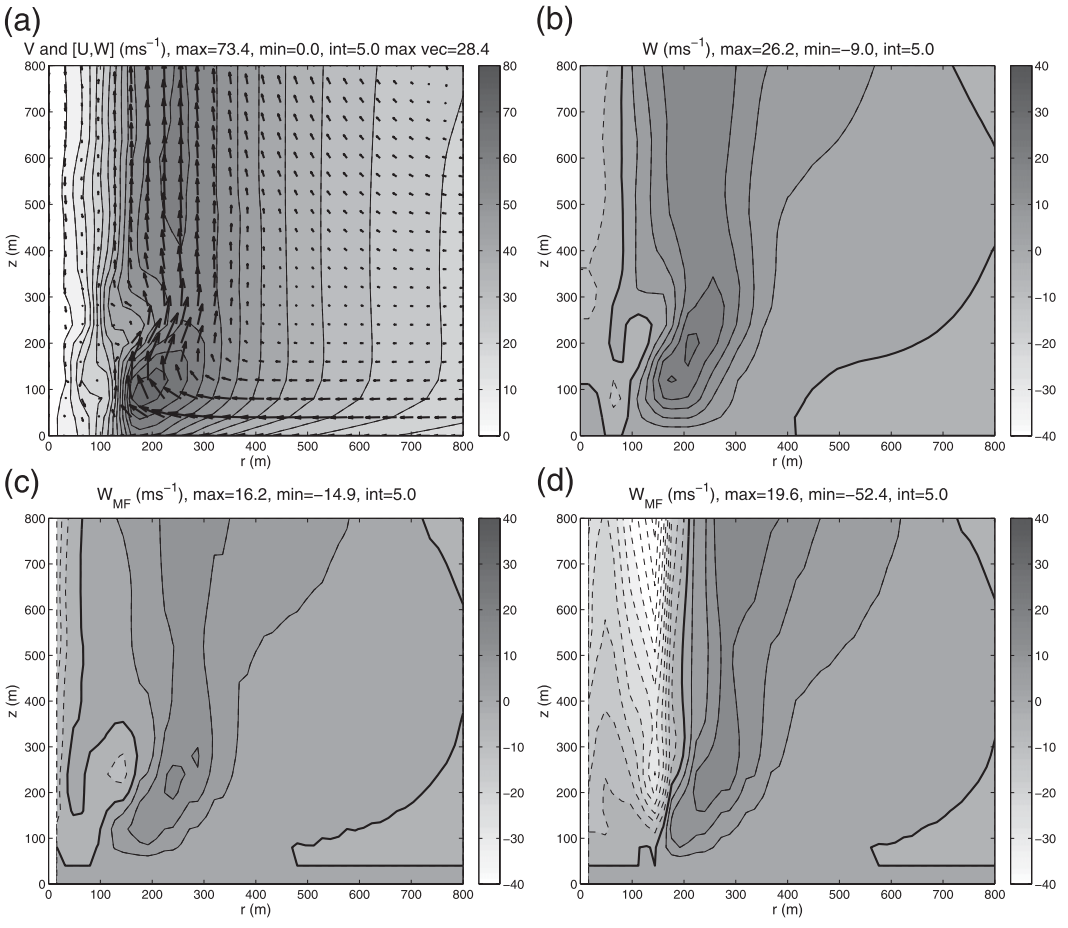

FIG. 7. Results using instantaneous wind fields from simulation BD: (a) axisymmetric V and meridional wind vectors $[U, W]$, (b) W, (c) W_{MF} integrated from $z = 40$ m, and (d) W_{MF} integrated from $z = 40$ m and using a biased U with $C_{max} = 4$ m s^{-1}.

in the boundary layer underneath strong vortices (e.g., Eliassen 1971; Kuo 1971; Kepert 2001; Foster 2009; Rotunno 2013). All of these solutions make various simplifications and approximations, but the details of the $U(z)$ profile are not nearly as important as the total inward mass flux of the boundary layer, which is much more constrained. Alternatively, more accurate, three-dimensional numerical simulations with realistic turbulence parameterizations could be used to develop empirical models of wind profiles in tornadic boundary layers.

The problem of accounting for centrifuging debris may be more challenging. Although Dowell et al. (2005) developed a method for computing the flow-relative outward motion of various classes (sizes) of debris, they also point out that the size distribution of debris can vary widely throughout the lifetime of each tornado, and presented evidence for such changes in the case of the same Spencer tornado moving across the town. As noted above, Wakimoto et al. (2012) used the numerical methods of Dowell et al. (2005) to estimate the outward wind bias caused by debris in a different case (Lagrange, Wyoming, 2009). The W fields they computed after correcting for this effect seemed much more realistic. However, we have no way of knowing if the new W fields are correct, and as the results in Figs. 4 and 6 show, the final solution is highly sensitive to the choice of the peak outward velocity bias (C_{max}). Future advances in technology may lead to a robust way of estimating the size distribution (or at least the peak of the distribution) for the lofted debris in tornadoes, which might lead to more reliable estimates of the outward wind bias.

In closing, we should emphasize that the criticisms of the methods and results described above do not apply specifically to the GBVTD technique. Rather we have shown that large errors can arise when using any Doppler radar wind analysis, even assuming that the method used—GBVTD or dual Doppler—is perfect.

The problems arise because of the large sensitivity of the calculation of W_{MF} to the unknown mass flux in the boundary layer and to the outward bias due to centrifuging debris.

Acknowledgments. The author would like to thank Dr. Karen Kosiba for providing the analyzed wind fields published in Kosiba and Wurman (2010). This work was supported in part by the National Science Foundation through Grant AGS-1132646 and by the University of Miami.

REFERENCES

Bell, M. M., and M. T. Montgomery, 2008: Observed structure, evolution, and potential intensity of category 5 Hurricane Isabel (2003) from 12 to 14 September. *Mon. Wea. Rev.,* **136,** 2023–2036.

Bluestein, H. B., A. L. Pazmany, J. C. Galloway, and R. E. Macintosh, 1995: Studies of the substructure of severe convective storms using a mobile 3-mm-wavelength Doppler radar. *Bull. Amer. Meteor. Soc.,* **76,** 2155–2169.

——, W.-C. Lee, M. Bell, C. C. Weiss, and A. L. Pazmany, 2003: Mobile Doppler radar observations of a tornado in a supercell near Bassett, Nebraska, on 5 June 1999. Part II: Tornado-vortex structure. *Mon. Wea. Rev.,* **131,** 2968–2984.

Dowell, D. C., C. R. Alexander, J. M. Wurman, and L. J. Wicker, 2005: Centrifuging of hydrometeors and debris in tornadoes: Radar-reflectivity patterns and wind-measurement errors. *Mon. Wea. Rev.,* **133,** 1501–1524.

Eliassen, A., 1971: On the Ekman layer in a circular vortex. *J. Meteor. Soc. Japan,* **49,** 784–789.

Fiedler, B. H., 1994: The thermodynamic speed limit and its violation in axisymmetric numerical simulations of tornado-like vortices. *Atmos.–Ocean,* **32,** 335–359.

——, 1998: Wind-speed limits in numerical simulated tornadoes with suction vortices. *Quart. J. Roy. Meteor. Soc,* **124,** 2377–2392.

——, 2009: Suction vortices and spiral breakdown in numerical simulations of tornado-like vortices. *Atmos. Sci. Lett.,* **10,** 109–114, doi:10.1002/asl.217.

Foster, R. C., 2009: Boundary-layer similarity under an axisymmetric, gradient wind vortex. *Bound.-Layer Meteor.,* **131,** 321–344.

Howard, L. N., and A. S. Gupta, 1962: On the hydrodynamic and hydromagnetic stability of swirling flows. *J. Fluid Mech.,* **14,** 463–476.

Kepert, J, 2001: The dynamics of boundary layer jets within the tropical cyclone core. Part I: Linear theory. *J. Atmos. Sci.,* **58,** 2469–2484.

Kosiba, K. A., and J. Wurman, 2010: Three-dimensional axisymmetric wind field structure of the Spencer, South Dakota, 1998 Tornado. *J. Atmos. Sci.,* **67,** 3074–3083.

——, R. J. Trapp, and J. Wurman, 2008: An analysis of the axisymmetric three-dimensional low level wind field in a tornado using mobile radar observations. *Geophys. Res. Lett.,* **35,** L05805, doi:10.1029/2007GL031851.

Kuo, H. L., 1971: Axisymmetric flows in the boundary layer of a maintained vortex. *J. Atmos. Sci.,* **28,** 20–41.

Lee, W.-C., and F. D. Marks, 2000: Tropical cyclone kinematic structure retrieved from single-Doppler radar observations. Part II: The GBVTD-simplex center finding algorithm. *Mon. Wea. Rev.,* **128,** 1925–1936.

——, and J. Wurman, 2005: Diagnosed three-dimensional axisymmetric structure of the Mulhall tornado on 3 May 1999. *J. Atmos. Sci.,* **62,** 2373–2393.

——, and M. M. Bell, 2007: Rapid intensification, eyewall contraction, and breakdown of Hurricane Charley (2004) near landfall. *Geophys. Res. Lett.,* **34,** L02802, doi:10.1029/2006GL027889.

——, B. J.-D. Jou, P.-L. Chang, and S.-M. Deng, 1999: Tropical cyclone kinematic structure retrieved from single-Doppler radar observations. Part I: Intepretation of Doppler velocity patterns and the GBVTD technique. *Mon. Wea. Rev.,* **127,** 2419–2439.

——, ——, ——, and F. D. Marks, 2000: Tropical cyclone kinematic structure retrieved from single-Doppler radar observations. Part III: Evolution and structures of Typhoon Alex (1987). *Mon. Wea. Rev.,* **128,** 3982–4001.

Leibovich, S., and K. Stewartson, 1983: A sufficient condition for the instability of columnar vortices. *J. Fluid Mech.,* **126,** 335–356.

Lewellen, D. C., W. S. Lewellen, and J. Xia, 2000: The influence of a local swirl ratio on tornado intensification near the surface. *J. Atmos. Sci.,* **57,** 527–544.

Lewellen, W. S., D. C. Lewellen, and R. I. Sykes, 1997: Large-eddy simulation of a tornado's interaction with the surface. *J. Atmos. Sci.,* **54,** 581–605.

Nolan, D. S., 2005: A new scaling for tornado-like vortices. *J. Atmos. Sci.,* **62,** 2639–2645.

——, 2012: Three-dimensional instabilities in tornado-like vortices with secondary circulations. *J. Fluid Mech.,* **711,** 61–100.

——, and B. F. Farrell, 1999: The structure and dynamics of tornado-like vortices. *J. Atmos. Sci.,* **56,** 2908–2936.

——, D. P. Stern, and J. A. Zhang, 2009: Evaluation of planetary boundary layer parameterizations in tropical cyclones by comparison of in-situ observation and high-resolution simulations. Part II: Inner-core boundary layer and eyewall structure. *Mon. Wea. Rev.,* **137,** 3675–3698.

Rotunno, R., 2013: The fluid dynamics of tornadoes. *Annu. Rev. Fluid Mech.,* **45,** 59–84.

Tanamachi, R. L., H. B. Bluestein, W.-C. Lee, M. Bell, and A. Pazmany, 2007: Ground-based velocity-track display (GBVTD) analysis of W-band Doppler radar data in a tornado near Stockton, Kansas, on 15 May 1999. *Mon. Wea. Rev.,* **135,** 783–800.

Wakimoto, R. M., P. Stauffer, W.-C. Lee, N. T. Atkins, and J. Wurman, 2012: Finescale structure of the LaGrange, Wyoming, tornado during VORTEX2: GBVTD and photogrammetric analyses. *Mon. Wea. Rev.,* **140,** 3397–3418.

Wurman, J., J. M. Straka, E. N. Rasmussen, M. Randall, and A. Zahrai, 1997: Design and deployment of a portable, pencil-beam, pulsed, 3-cm Doppler radar. *J. Atmos. Oceanic Technol.,* **14,** 1502–1512.

——, Y. Richardson, C. Alexander, S. Weygandt, and P. F. Zhang, 2007: Dual-Doppler analysis of wind and vorticity budget terms near a tornado. *Mon. Wea. Rev.,* **135,** 2392–2405.

——, K. Kosiba, P. Markowski, Y. Richardson, D. Dowell, and P. Robinson, 2010: Finescale single- and dual-Doppler analysis of tornado intensification, maintenance, and dissipation in the Orleans, Nebraska, supercell. *Mon. Wea. Rev.,* **138,** 4439–4455.

Zhang, D.-L., Y. Liu, and M. K. Yau, 2001: A multiscale numerical study of Hurricane Andrew (1992). Part IV: Unbalanced flows. *Mon. Wea. Rev.,* **129,** 92–107.

Zhang, J. A., R. F. Rogers, D. S. Nolan, and F. D. Marks, 2011: On the characteristic height scales of the hurricane boundary layer. *Mon. Wea. Rev.,* **139,** 2523–2534.